EPELBOIN, Y. (1979). *Acta Cryst.* A**35**, 38–44.
HEAD, A. K., HUMBLE, P., CLAREBROUGH, L. M., FORWOOD, C. T. & MORTON, A. J. (1973). *Defects in Crystalline Solids.* Vol. 7. Amsterdam: North-Holland.
ISHIDA, H., MIYAMOTO, N. & KOHRA, K. (1976). *J. Appl. Cryst.* **9**, 240–241.
JENKINSON, A. E. & LANG, A. R. (1962). *Direct Observations of Imperfections in Crystals*, pp. 471–495. New York: Interscience.
KATAGAWA, T., ISHIKAWA, H. & KATO, N. (1975). *Acta Cryst.* A**31**, S246–S247.
KATO, N., KATAGAWA, T. & USAMI, K. (1967). *Adv. X-ray Anal.* **10**, 46–66.
KIMERLING, L. C., LEAMY, H. J. & PATEL, J. R. (1977). *Appl. Phys. Lett.* **30**, 217–219.
MAHER, D. M., STAUDINGER, A. & PATEL, J. R. (1976). *J. Appl. Phys.* **47**, 3813–3825.
PATEL, J. R. & AUTHIER, A. (1975). *J. Appl. Phys.* **46**, 118–125.
PATEL, J. R., JACKSON, K. A. & REISS, H. (1977). *J. Appl. Phys.* **48**, 5279–5288.
PATEL, J. R., WONSIEWICZ, B. C. & FREELAND, P. E. (1979). In preparation.
TAKAGI, S. (1962). *Acta Cryst.* **15**, 1311–1312.
WONSIEWICZ, B. C. & PATEL, J. R. (1976). *J. Appl. Phys.* **47**, 1837.

Acta Cryst. (1979). A**35**, 28–37

Dynamical Theory for Electron Scattering from Crystal Defects and Disorder*

BY J. M. COWLEY AND P. M. FIELDS

Department of Physics, Arizona State University, Tempe, Arizona 85281, *USA*

(*Received* 3 *April* 1978; *accepted* 5 *July* 1978)

Abstract

Dynamical diffraction calculations have been made by use of the periodic-continuation assumption for the diffuse scattering in electron diffraction patterns and for electron microscope images of single split interstitials in gold crystals for thicknesses up to 200 Å in order to demonstrate the strong fluctuations of scattering with thickness. The diffuse scattering from distributions of defects in crystals, described in terms of correlation functions, can be written in terms of 'dynamical factors' for each type of individual defect. These dynamical factors multiply the same Fourier transforms of correlation functions as are used in kinematical theory to give the effect of dynamical scattering on the diffraction intensities. Calculations of dynamical factors have been made by multi-slice dynamical diffraction methods for unit changes in atomic scattering factors and for atom displacements in gold and aluminum crystals in [001] orientation for thicknesses up to 100 Å. With increasing thickness the dynamical factors show rapidly reducing fluctuations with crystal thickness and become more nearly isotropic except for the effects of Kikuchi bands which are seen to develop.

* This paper was presented, by invitation, at the ACA Dynamical Diffraction Symposium held at the University of Oklahoma, 22 March 1978, honoring Paul P. Ewald on the occasion of his ninetieth birthday.

1. Introduction

Difficulties arise in the evaluation of electron scattering from defects and disorder in crystals because of the strong dynamical diffraction effects occurring even in very thin samples. While it is possible to write formal expressions for scattered amplitudes which are sufficiently accurate for the interpretation of any forseeable experimental observations with fast electrons (energy greater than about 20 keV), it is not in general feasible to make accurate calculations of the dynamical scattering effects for both the sharp Bragg reflections and the continuous background of diffuse scattering in diffraction patterns. The incentive to find approximate methods to deal with particular experimental situations has been considerable because of the significance of electron scattering methods for the study of perturbations of the periodicity of crystals, but as the power of the experimental methods has been increased the requirements for better approximations in the theoretical modelling have also been increased.

The use of a column approximation with, usually, a two-beam approximation and considerations limited to Bragg reflection amplitudes has served for much of the electron microscope study of dislocations and other extended crystal defects with medium-resolution imaging (10 Å or greater) for many years (Hirsch, Howie, Nicholson, Pashley & Whelan, 1965). Improved

00567-7394/79/010028-10$01.00

approximations to overcome the limitations of the column approximation were evolved to account for observations with improved resolution, following Takagi (1962), but these still included only the Bragg reflections or else introduced the diffuse scattering amplitudes only in a severely limited form (see Howie & Basinski, 1968).

For the resolutions in the range of 2 to 3 Å or even better, now being achieved or being contemplated for the near future, none of these previously applied approximations can be adequate since scattering from the individual displaced atoms or from individual substitutional atoms or vacancies can contribute appreciably to the image. It is no longer sufficient to consider slowly varying strain fields as the origin of the image contrast. Under these circumstances the scattering amplitudes must be calculated in terms of the scattering from all atoms considered individually. Some calculations along these lines have been made using a kinematical approximation for the diffuse scattering amplitudes (Krakow, 1976; Kuan & Sass, 1976). This is justifiable in the case of X-ray diffraction but is rarely so for electron diffraction.

The only technique which takes dynamical diffraction effects fully into account makes use of the periodic continuation approximation whereby the defect is assumed to be repeated regularly in two dimensions to form a two-dimensional superlattice for which the diffraction intensities and image contrast can be calculated by use of the multi-slice n-beam dynamical diffraction computer programs used in calculations for perfect crystals (see Cowley, 1975). Calculations have been made in this way by Fields & Cowley (1978) for split interstitials in f.c.c. metals, by Spence (1978) for dislocation cores and by Iijima & O'Keefe (1979) for defects in complex oxide phases. In this paper we present further calculations on the images and diffraction intensities from split interstitials without relaxation, in order to illustrate more fully the effect on the observations of crystal thicknesses in the experimentally accessible range.

The observation of diffuse scattering intensities in electron diffraction patterns has become an important technique for the detection and characterization of disorder and the statistics of defect arrays in crystals (Cowley, 1971). However, the method has been limited by the difficulty of assessing the nature and magnitude of dynamical diffraction effects on the diffuse scattering.

The essential difficulty in the computer simulation of dynamical diffuse scattering from distributions of defects arises because one cannot assume the linear superposition of scattered waves from individual atoms which is the basis for the correlation function formulation of the kinematical approximation used for X-ray diffraction studies. The electron diffraction pattern amplitude is given by the Fourier transform of the wave function at the exit face of the crystal which is produced by the complicated multiple-scattering processes within the crystal. The elastic diffuse scattering intensity is a measure of the statistical correlations of deviations of this wave function from the periodic average component of the complex wave amplitude. In general this shows little relationship with, and is not directly derivable from, the statistics of the variations of deviations from the periodic average potential or electron density distributions. As pointed out by Cowley & Murray (1968) it is not possible to describe the scattering, even from a thin layer using the phase-object approximation, in terms of the short-range-order coefficients which are sufficient to describe the kinematical diffraction intensities. Higher-order correlation coefficients must be invoked.

In order to make some reasonable estimates of dynamical effects on diffuse scattering, Gjønnes (1966) introduced the method, used by Fisher (1965) and Gjønnes & Watanabe (1966), whereby each individual thin slice of a crystal, perpendicular to the incident beam, is assumed to produce a diffuse scattering distribution equivalent to that for the kinematical scattering from the average defect distribution. The calculation of diffuse scattering then proceeds by the 'three-region' method as suggested in Fig. 1. For diffuse scattering in the nth slice of a crystal, it is assumed that in region 1, slices 1 to $n-1$, the incident beam undergoes n-beam dynamical scattering by the average lattice. Only the Bragg reflections with reciprocal-lattice vectors $\mathbf{h}$ are considered, although an absorption coefficient may be included to allow for the energy losses by diffuse scattering. In region 2 each incident Bragg reflected beam gives rise to diffuse scattering. In region 3 each diffusely scattered beam with initial direction $\mathbf{h}_i + \Delta$ undergoes n-beam dynamical scattering, interacting through Bragg reflections with all other scattered beams $\mathbf{h}_i + \Delta$. The amplitudes $\Psi_n(\mathbf{h} + \Delta)$ at the exit face are thus calculated and the observed intensity is then given by

$$I(\mathbf{h} + \Delta) = \sum_n |\Psi_n(\mathbf{h} + \Delta)|^2, \qquad (1)$$

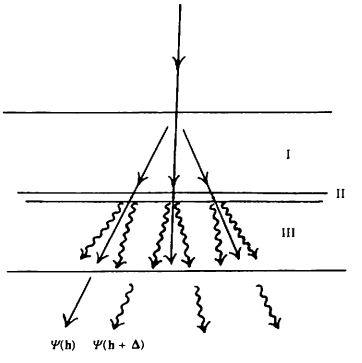

Fig. 1. Diagram suggesting the three-region scheme for dynamical diffuse calculations.

or

$$I(\mathbf{h}+\mathbf{\Delta}) = |\sum_n \Psi_n(\mathbf{h}+\mathbf{\Delta})|^2, \qquad (2)$$

depending on whether the scattering from all slices is considered to be independent and uncorrelated, as in (1), or is assumed to be correlated, as in (2). Intermediate degrees of correlation between slices are also possible (Cowley & Pogany, 1968).

Calculation by this method assumes that the diffuse scattering is weak so that double diffuse scattering can be ignored. It does, however, include the full dynamical diffraction effects on the diffuse scattering due to the interactions of Bragg reflected beams. The method has been used effectively by Doyle (1969, 1971) for the calculation of thermal diffuse scattering and plasmon scattering in thin crystals. The thickness of crystal for which Doyle could make his calculations was strictly limited by the large amount of computing involved in evaluating (1) or (2) for a sufficient range of $\mathbf{\Delta}$ values, even for one-dimensional cases.

It is our purpose in the latter part of this paper to show that under certain well defined conditions it is possible to avoid the essential assumptions of this method of Gjønnes and express the dynamical diffuse scattering in terms of a 'dynamical factor' which multiplies the kinematical diffuse scattering intensity function. Calculations of the dynamical-factor functions can be made by use of the same assumptions of periodic continuation as in the case of individual defect diffraction patterns and images.

2. Calculations for individual split interstitials

Following the methods of Fields & Cowley (1978) further calculations have been made for the particular case of a [100] split interstitial in a gold crystal without relaxation of neighboring atoms with the incident beam in the [001] direction, in order to determine in more detail the nature of the variation of the image and the diffraction pattern with thickness and to provide a better basis for comparison with the calculations relevant to statistical distributions of defects. The accelerating voltage was taken as 1 MeV and the objective aperture, $u_o = 0{\cdot}465$ Å^{-1}, was chosen to just exclude the innermost Bragg reflections, namely the four 200-type reflections.

In the first slice of crystal, split interstitials were assumed to occur at intervals of 8·1 Å in each direction so that the superlattice cell chosen was 2 × 2 perfect-crystal unit cells. This perturbed slice was followed by from 1 to 100 perfect-crystal slices each 2 Å thick. To generate the phase grating approximation for the initial slice 2997 Fourier coefficients ('beams') were used and 1369 beams were used for the iterative multi-slice calculations.

For very thin crystals (less than about 8 Å thick) the diffraction pattern resembles the kinematic, with diffuse scattering bands of intensity distribution

$$I(u) = [2\cos 2\pi u(a/4) - 1]^2, \qquad (3)$$

since the deviation from the perfect-crystal lattice is minus one atom at 0,0 and plus one atom at $a/4$,0 and $-a/4$,0, *i.e.* odd-order bands are strong and even-order bands are weak as in Fig. 2(*a*). The relative intensities of diffuse bands are reversed for a thickness of about 20 Å and reverse again for each subsequent 20 Å increase of thickness. In Fig. 3(*a*) the intensities of diffuse scattering at the peaks of the zero- and first-order bands are plotted against thickness, showing their

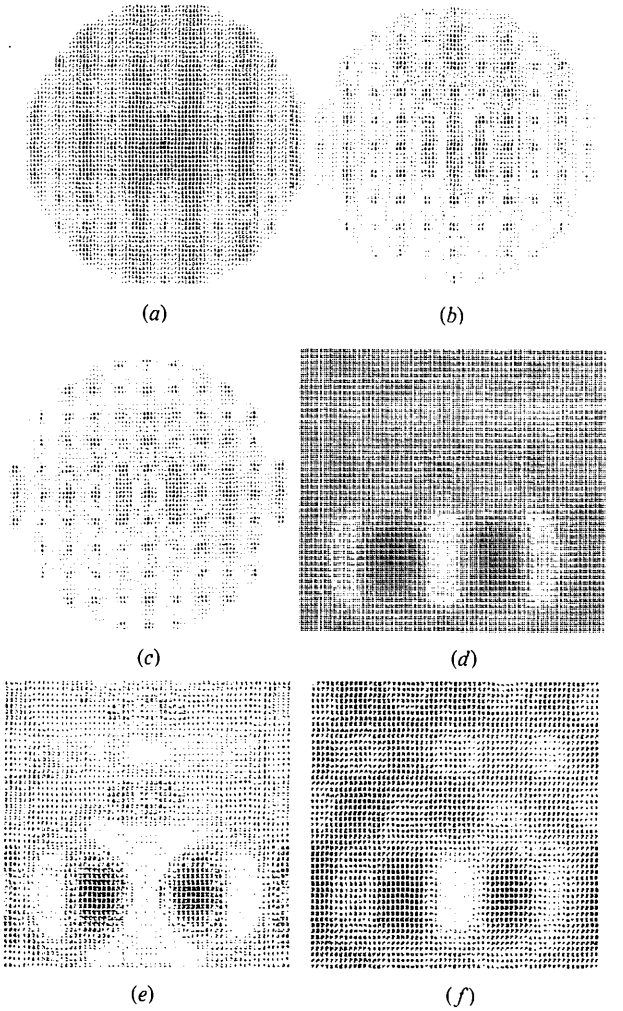

Fig. 2. Computer print-out of intensities, on a logarithmic scale, for the electron diffraction pattern for a single [100] split interstitial, without relaxation, in a gold single crystal for thicknesses (*a*) 4 Å, (*b*) 12 Å and (*c*) 120 Å; electron energy 1 MeV, incident direction [001], h axis horizontal. (*d*), (*e*) and (*f*) are calculated images for the same thicknesses, with a defocus of −470 Å and objective aperture size $u_o = 0{\cdot}49$ Å^{-1}, $C_s = 1{\cdot}8$ mm.

slowly damped oscillations and the reversals of contrast up to a thickness of 200 Å where the fluctuations of intensity with thickness are still of the order of 35%. For comparison, Fig. 3(*b*) shows the variation with thickness of the 000, 200 and 400 Bragg reflections. Fig. 2(*b*) shows a mapping of the diffuse scattering distribution for 12 Å thickness for which the even-ordered diffuse maxima are larger in the center of the pattern. With increasing thickness the alternation of strong and weak diffuse bands across the pattern becomes less distinct, particularly for the outer parts of the pattern. Fig. 2(*c*) is for a thickness of 120 Å for which the alternation of strong and weak bands is not so evident but the even-order bands are weaker. This effect is shown more quantitatively in Fig. 4 which compares the intensity distribution across the bands for thicknesses of 20 and 100 Å. The variation of the diffraction pattern with thickness is much less obvious for aluminum for which the kinematical form of the pattern, similar to Fig. 2(*a*), persists to much greater thicknesses, although the details of the intensity distribution are appreciably modified.

The images of the split interstitial for thicknesses 4, 12 and 120 Å are shown in Fig. 2(*d*), (*e*) and (*f*). The defocus was −470 Å, close to the Scherzer optimum defocus, and the objective aperture, $u_o = 0{\cdot}49$ Å^{-1}, was chosen just to exclude the inner Bragg reflections. In each case the positions of the added atoms are indicated clearly by dark spots. For some thicknesses, Fig. 2(*d*) and (*f*), the position of the missing atom is indicated by a white spot but for other thicknesses, Fig. 2(*e*), this white spot is split or obscured. The main features of the image appear to fluctuate with thickness much less than those of the diffraction pattern. The image contrast defined by $(I_{max} - I_{min})/I_{ave}$ varied with thickness in the range of 15 to 25%.

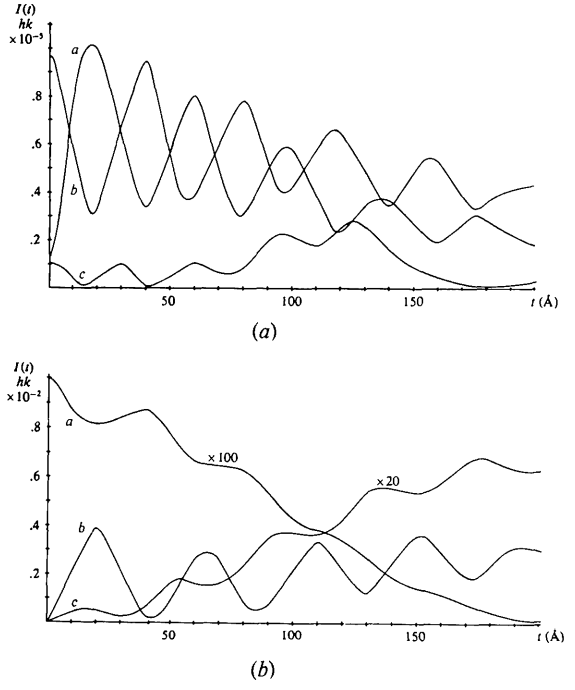

Fig. 3. Variation with thickness of (*a*) the intensities at the maxima of the diffuse bands of Fig. 2(*a*) to (*c*) [*h*,*k* coordinates 0,1 for curve *a*, 2,1 for curve *b* and 6,1 for curve (*c*), relative to normal Au unit cell], and (*b*) the sharp Bragg reflections of Figs. 2(*a*) to (*c*) (*h*,*k* coordinates 0,0 for curve *a*, 4,0 for curve *b*, 2,0 for curve *c*). The scale is multiplied by the indicated factors for curves *a* and *c*.

3. Diffuse scattering by distributions of defects

We wish to treat the case of a short-range ordering of individual deviations from an average periodic crystal structure when the density of defects is high and the observed diffraction pattern comes from a spatial or time average from a large number of defects. We include, for example, thermal diffuse scattering and Huang scattering from correlated displacements of individual atoms from their lattice sites, but also short-range-order diffuse scattering from solid solutions of binary alloys, or more complicated systems, where the occupancy of a lattice site by a particular atomic species represents a deviation from the averaged site occupancy of the periodic average structure. Similarly we include point defects such as interstitials or vacancies, or clusters of these defects, with the associated atom displacements which constitute the 'relaxation' of the surrounding structure. However, we adopt a new approach in which we do not include these recognized forms of individual defects as such. Instead we subdivide the defects into elementary 'unit' deviations from the periodic structure, distinguished by the form of their contributions to the diffuse scattering. Thus the subtraction of an atom to form a vacancy is described in terms of a multiple of a unit deviation which represents unit change in scattering amplitude (potential) of an atom, while the relaxation of the lattice is described by ascribing to each atom position an

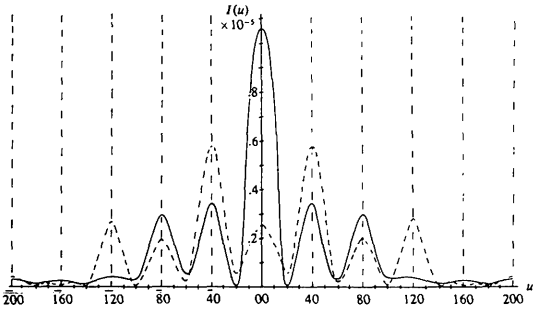

Fig. 4. Variation of intensity across the diffraction pattern from split interstitial in gold (Fig. 2) for thicknesses 20 Å (full line) and 100 Å (dashed line). The vertical dashed lines represent the sharp Bragg reflections. Coordinates refer to the superlattice unit cell.

appropriate multiple of the unit change in potential corresponding to a small atom displacement in the appropriate direction.

In order to clarify our approach we first rewrite the standard kinematical formulas for scattering from such a defect system in a form which is more appropriate for extension to dynamical scattering. In the kinematical approximation the potential distribution of the crystal, $\varphi(\mathbf{r})$, can be written in terms of the periodic, average potential $\bar{\varphi}(\mathbf{r})$ and the non-periodic deviation from the average, $\Delta\varphi(\mathbf{r})$:

$$\varphi(\mathbf{r}) = \bar{\varphi}(\mathbf{r}) + \Delta\varphi(\mathbf{r}). \tag{4}$$

Then the scattered intensity can be written (see, for example, Cowley, 1975) as

$$I(\mathbf{u}) = |\bar{F}(\mathbf{u})|^2 + |\Delta F(\mathbf{u})|^2, \tag{5}$$

where $\mathbf{u}$ is the reciprocal-space vector and $F(\mathbf{u})$ and $\Delta F(\mathbf{u})$ are the Fourier transforms of $\bar{\varphi}$ and $\Delta\varphi$ and the two terms on the right-hand side of (5) represent the sharp Bragg reflections and the diffuse scattering respectively. The average potential, $\bar{\varphi}(\mathbf{r})$, may perhaps be understood as the inverse Fourier transform of $\bar{F}(\mathbf{u}) = F(\mathbf{u}) \sum_{\mathbf{h}} \delta(\mathbf{u} - \mathbf{h})$, where $\mathbf{h}$ is a reciprocal-lattice vector.

We now describe $\Delta\varphi$ in terms of the various possible types of deviations from the average lattice, the type being indicated by the superscript n:

$$\Delta\varphi(r) = \sum_n \sum_i C_i^n \, \Delta\varphi_i^n * \delta(\mathbf{r} - \mathbf{r}_i). \tag{6}$$

For a substitution of one atom for another, or the occupancy of a site in a disordered alloy by one or another type of atom, $\Delta\varphi_i^n$ would have the form $\varphi_1(r) - \varphi_2(r)$ where φ_1 and φ_2 are the potential distributions for the types of atom. The constants C_i^n then may be positive or negative and may have any magnitude to represent the presence of any type of atom or a vacancy. For atom displacements ε in the $\mathbf{x}$ direction, for example, $\Delta\varphi_i^n$ will have the form $\varphi_1(\mathbf{r}) - \varphi_1(\mathbf{r} - \varepsilon\mathbf{x})$, which is approximately of the form $\varepsilon\varphi_1'(\mathbf{r})$, where $\varphi_1'(\mathbf{r})$ represents the derivative with respect to x, and the constants C_i^n will depend on the magnitude and sign of the displacements and the nature of the atoms involved.

The diffuse scattering intensity is then written

$$I_d(\mathbf{u}) = |\Delta F(\mathbf{u})|^2 = \sum_m \sum_n \sum_k \sum_j C_k^n \, \Delta\Phi_k^n(\mathbf{u}) . C_j^m \, \Delta\Phi_j^{m*}(\mathbf{u}) \times \exp\{2\pi i \mathbf{u} . (\mathbf{r}_k - \mathbf{r}_j)\}. \tag{7}$$

Putting $\mathbf{r}_k - \mathbf{r}_j = \mathbf{r}_i$ and taking each site as origin in turn we obtain the expression in terms of the correlation coefficients $\langle C_o^m \, C_i^n \rangle$ where the angle brackets represent a spatial averaging:

$$I_d(\mathbf{u}) = N \sum_m \sum_n \Delta\Phi^m(\mathbf{u}) \, \Delta\Phi^n(u) \sum_i \langle C_o^m \, C_i^n \rangle \times \exp\{2\pi i \mathbf{u} . \mathbf{r}_i\}. \tag{8}$$

If only one type of defect is present, as in the case of short-range order in binary-alloy solid solutions, with no size effect or thermal displacements of the atoms, this becomes

$$I_d(u) = N |\Delta\Phi^1(u)|^2 \sum_i \langle C_o \, C_i \rangle \exp\{2\pi i \mathbf{r}_i\}, \tag{9}$$

which is the standard expression (see Cowley, 1975, p. 359).

The main complication of dynamical scattering lies in the fact that instead of considering the three-dimensional Fourier transform of the potential distribution as in (4) we must consider the two-dimensional Fourier transform $\Psi(uv)$ of the wave function at the exit face of the crystal $\psi(xy)$;

$$I(u,v) = |\bar{\Psi}(uv)|^2 + |\Delta\Psi(uv)|^2. \tag{10}$$

The contribution of a deviation from the average structure at a crystal lattice site to the deviation $\Delta\Psi(u,v)$ depends not only on the nature and magnitude of the deviation but also on its position within the crystal, especially in the incident-beam direction, because of the strong dynamical diffraction effects undergone by the scattered wave as it progresses through the crystal. This contribution is therefore characterized by an index t to denote depth in the crystal in the beam direction or, in the language of the multi-slice method of computation, by a slice number.

A small deviation from the average potential distribution of type n at site i in slice t of the crystal may be assumed to give a deviation $\Delta\Psi_i^{n,t}(uv)$ in the Fourier transform of the wave function at the exit face of the crystal. A deviation which is C_i times as large will give a deviation $C_i \Delta\Psi_i^{n,t}(uv)$ only if the total deviation from the averaged potential is sufficiently small, *i.e.* if a kinematical approximation can be used for the scattering from the individual defect. For the moment we assume this case of small local deviations from the average potential, but will consider the breakdown of this approximation at a later stage.

If we also make the assumption that deviations from the average structure are independent in different slices of the crystal, the diffracted intensity can be written, by analogy with (7), as

$$I_d(u,v) = \sum_t \sum_m \sum_n \sum_k \sum_j C_k^{n,t} \, C_j^{m,t} \, \Delta\Psi_k^{n,t}(uv) \, \Delta\Psi_j^{m,t*}(uv) \times \exp\{2\pi i [u(x_k - x_j) + v(y_k - y_j)]\}. \tag{11}$$

On the assumption that all appreciable correlation coefficients $\langle C_k^{nt} C_j^{mt} \rangle$ are confined to one slice thickness we may express this in terms of general correlation coefficients $\langle C_k^n C_j^m \rangle$ and use three-dimensional vectors **u**,**r**. Because the scattering is given by a two-dimensional section of a three-dimensional distribution, we can write it in terms of these three-dimensional vectors, in analogy with (9):

$$\begin{aligned} I_d(uv) &= N \sum_t \sum_m \sum_n \Delta\Psi^{n,t}(\mathbf{u})\, \Delta\Psi^{m,t^*}(\mathbf{u}) \\ &\quad \times \sum_i \langle C_o^n C_i^m \rangle \exp\{2\pi i \mathbf{u}.\mathbf{r}_i\} \\ &= N \sum_m \sum_n \left[\sum_t \Delta\Psi^{m,t}(\mathbf{u}).\Delta\Psi^{m,t^*}(\mathbf{u}) \right] \\ &\quad \times \sum_i \langle C_o^n C_i^m \rangle \exp\{2\pi i \mathbf{u}.\mathbf{r}_i\}. \end{aligned} \tag{12}$$

If there is only one type of defect present this reduces to

$$I_d(\mathbf{u}) = N \sum_t |\Delta\Psi^n(\mathbf{u})|^2 . \sum_i \langle C_o\, C_i \rangle \exp\{2\pi i(\mathbf{u}.\mathbf{r}_i)\}. \tag{13}$$

Here the summation over t takes the place of $|\Delta\Phi(u)|^2$ in (9) and may be regarded as a 'squared dynamical structure factor', or 'dynamical factor' for short, which multiplies the second term which is identical with that in the kinematical case.

For more than one type of defect, the expression becomes more complicated. For example, for types 1 and 2 present (*e.g.* atomic replacements and atomic displacements in one direction), equation (12) becomes

$$\begin{aligned} I_d(\mathbf{u}) &= \sum_t |\Delta\Phi^{1,t}(\mathbf{u})|^2 . \sum_i \langle C_o^1 C_i^1 \rangle \exp\{2\pi i \mathbf{u}.\mathbf{r}_i\} \\ &\quad + \sum_t |\Delta\Phi^{2,t}(\mathbf{u})|^2 . \sum_i \langle C_o^2 C_i^2 \rangle \exp\{2\pi i \mathbf{u}.\mathbf{r}_i\} \\ &\quad + \sum_t [\Delta\Phi^{1,t}(\mathbf{u}).\Delta\Phi^{2,t^*}(\mathbf{u}) + \text{c.c.}] \\ &\quad \times \sum_i \langle C_o^1 C_i^2 \rangle \exp\{2\pi i \mathbf{u}.\mathbf{r}_i\}. \end{aligned} \tag{14}$$

Thus with only one sort of defect present it is necessary to calculate only one dynamical factor which then multiplies the kinematical scattering expression based on the correlation coefficients or short-range-order parameters of the defect arrangement. This dynamical factor will depend on crystal thickness and orientation but will, in general, be a slowly varying function. It needs to be calculated only once to allow the diffuse scattering distribution to be calculated for any assumptions as to the degree or extent of short-range ordering for which the initial assumptions apply. For two types of defect, three dynamical factors will be needed for each crystal orientation and thickness, and so on.

For atom displacements, since the deviation from the average structure does not have the symmetry of the average structure, the dynamical factor will, in general, be different for each direction of displacement perpendicular to the incident beam. However, to a good approximation it will usually be possible to express any displacement perpendicular to the incident beam in terms of a sum of displacements in two perpendicular directions. For crystals having fourfold axes in the incident-beam direction the two dynamical factors then needed will be identical apart from a 90° rotation. It will be necessary to calculate only two dynamical factors: one for the first two terms of (14) and one for the third term. This type of aproximation will be particularly good for reasonably thick crystals since, as we will show later, the dynamical factors tend to become increasingly isotropic with increasing crystal thickness.

4. The calculation of dynamical factors

In order to investigate the feasibility of calculating dynamical factors and to gain an impression of the form of these functions and the extent to which they vary with crystal thickness and other parameters, we have made some calculations for the relatively simple cases of the face-centered cubic metals aluminum and gold. The same assumptions of periodic continuation could be made as in the case of the calculations of diffuse scattering from individual defects. For each type of defect the function $\Delta\Psi^t(\mathbf{u})$ is calculated for a small deviation from the average lattice at one atomic site in the slice number t in the crystal and the intensity distribution $|\Delta\Psi^t(\mathbf{u})|^2$ is found. Then the dynamical factor is given by summing for all t up to the maximum corresponding to the crystal thickness.

The superlattice unit cell chosen in each case had twice the dimensions of the perfect-crystal unit cell. To generate the phase grating for an individual slice 2997 beams were used, and 529 beams were used in the iterative multi-slice calculation with a slice thickness of 4 Å. For the four sets of calculations, giving dynamical factors for thicknesses of up to 100 Å for vacancies and for atom displacements in gold and aluminum, the total computing time on a Univac 1110 computer was 8 h. For the vacancy calculations, the unit defect was taken to be 0·1 atoms of gold or 1·0 atoms of aluminum. For the displacement calculations the unit defect corresponded to the shifting of one atom by 0·05 Å.

Computer print-out maps of the dynamical factors are shown in Figs. 5 to 8. A logarithmic scale has been used. The regularly spaced black dots represent the

positions of the sharp Bragg reflections, $2h,2k,0$ of the unperturbed structures. Contour lines of diffuse scattering intensity have been drawn to emphasize the form of the distributions. More quantitative representations of sections of these maps are given by plots of intensity against distance across the middle of the maps in Figs. 9 to 12.* In these plots the vertical lines represent the sharp Bragg reflections. In each case diffuse intensity curves are given for two thicknesses: (*a*) 12 Å and (*b*) 40 Å. For the latter curve in each case the vertical scale has been adjusted by multiplying by the factor indicated.

For the vacancy in aluminum, Figs. 5 and 9,* the diffuse scattering retains the circular symmetry of the kinematical scattering case and has an almost monotonic fall-off with scattering angle. For increasing thickness the distribution becomes broader with only minor changes in shape.

In the case of gold (Figs. 6 and 10) the stronger dynamical scattering effects are evident. Even for 12 Å thickness [Fig. 6(*a*) and Fig. 10, curve (*a*)] there is an inversion of the kinematical distribution for small scattering angles although the distribution remains roughly isotropic. For greater thicknesses, as in Fig. 6(*b*) for 84 Å and Fig. 6(*c*) for 100 Å, strong bands of diffuse scattering develop along the [100] and [010] directions with weaker bands along [110]. These are the well known Kikuchi-band or 'channelling' effects.

For unit displacements the dynamical factor plots for thin crystals have the typical double-maximum appearance, as for kinematical scattering, with weak scattering along a line perpendicular to the displacement [Figs. 7(*a*) and 11 for Al; Figs. 8(*a*) and 12 for Au]. However, even for 12 Å thickness the scattering is asymmetric, especially for gold. For an asymmetric displacement, the center of symmetry required for kinematical scattering no longer appears. For greater thicknesses the dynamical factors rapidly become more isotropic with a reduction or even elimination of the trough perpendicular to the displacement direction, as seen by Figs. 7(*b*) for aluminum and 8(*b*) for gold calculated for 84 Å and by the curves (*b*) in Figs. 11 and 12 calculated for 40 Å thickness.

For aluminum the variation of the dynamical factor with thickness is smooth and monotonic as illustrated in Figs. 13* and 15* which show the variations for the points $h,k = 3,0$ (curve *a*) and 10,0 (curve *b*) where these coordinates refer to the superlattice unit cell. For gold, as shown by Figs. 14 and 16, there are initially strong fluctuations of the dynamical factor with

* Figs. 9, 13 and 15 have been deposited with the British Library Lending Division as Supplementary Publication No. SUP 33901 (4 pp.). Copies may be obtained through The Executive Secretary, International Union of Crystallography, 5 Abbey Square, Chester CH1 2HU, England.

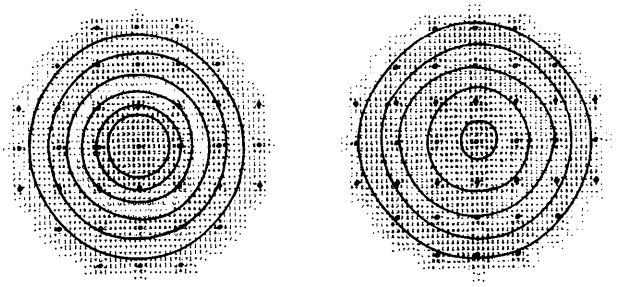

(*a*) (*b*)

Fig. 5. Computer print-out map of dynamical factor for unit vacancy defects in aluminum crystal, [001] orientation; logarithmic scale, diffuse intensities contoured, Bragg reflections indicated by black dots. Thicknesses (*a*) 12 Å and (*b*) 84 Å.

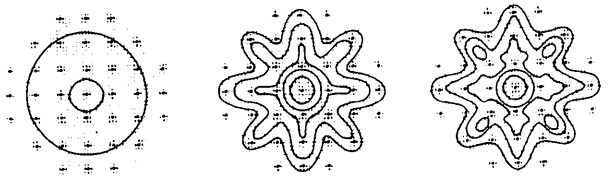

(*a*) (*b*) (*c*)

Fig. 6. As for Fig. 5 but for gold crystal. Thicknesses (*a*) 12 Å, (*b*) 84 Å and (*c*) 100 Å.

* See previous footnote.

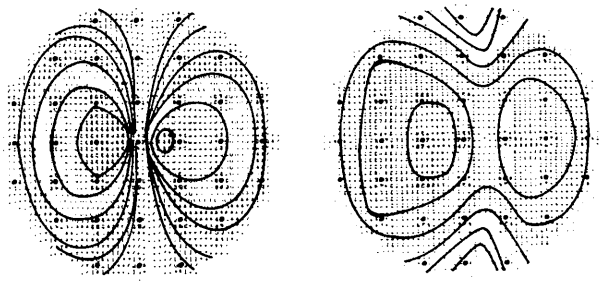

(*a*) (*b*)

Fig. 7. As for Fig. 5 but for unit displacement defects in aluminum. Thicknesses (*a*) 12 Å and (*b*) 84 Å.

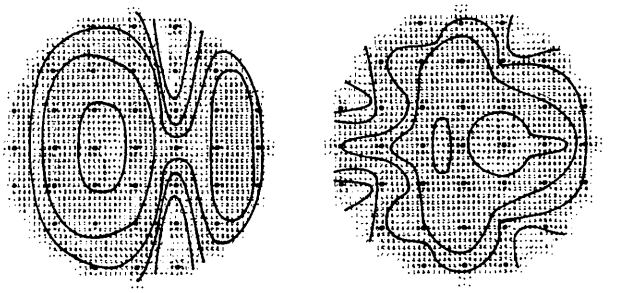

(*a*) (*b*)

Fig. 8. As for Fig. 7 but for gold crystal. Thicknesses (*a*) 12 Å and (*b*) 84 Å.

thickness, almost as large as those for a single interstitial (Fig. 3*a*), but these fluctuations are rapidly damped and for thicknesses greater than about 75 Å the variation with thickness appears to become nearly monotonic.

5. Conclusions

It is evident from the results we have presented that the dynamical scattering effects on diffuse electron scattering are strong, especially for heavy-atom materials, even at high voltages. The particular orientation chosen, with the incident beam parallel to the cubic unit-cell axis, is one of strong *n*-beam dynamical interaction but, as shown by Fig. 3(*b*), cannot be classed with the cases of very strong interaction in which the incident beam loses most of its intensity in its first oscillation for thicknesses of less than 50 Å (see, for example, Fejes, Iijima & Cowley, 1973). The dynamical effects would be stronger if, for example, the incident beam were tilted to satisfy the Bragg condition for the 200, 020 and 220 reflections. The axial orientation is appropriate, however, in that it is the optimum for the imaging of defects and it is also the orientation most commonly chosen for observing diffuse scattering effects.

For individual interstitials in gold the intensities of the diffuse bands oscillate rapidly with thickness and the oscillations persist into the thickness region of experimental significance. Single-crystal gold films a few hundred ångströms thick are readily made but it is very difficult to prepare films less than 100 Å thick.

Usually, experimental conditions will be such as to reduce the effects of the thickness dependence. Variations of crystal thickness due to surface steps will tend to smooth out the intensity oscillations. Also, in order to obtain diffraction from a region small enough to allow the diffraction effects of a single interstitial to be seen, a convergent incident beam will be required, as in a scanning transmission electron microscope, and the integration of intensities over the incident-beam direction will smooth out the thickness fluctuations.

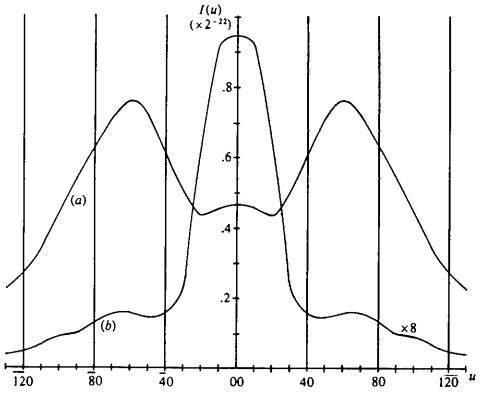

Fig. 10. Profile of intensity distribution across dynamical factor for vacancy defects in gold (*cf* Fig. 6). Thicknesses (*a*) 12 Å and (*b*) 40 Å. The vertical lines represent the sharp Bragg reflection positions. The vertical scale on curve (*b*) is multiplied by a factor of 8. Coordinates refer to the superlattice unit cell.

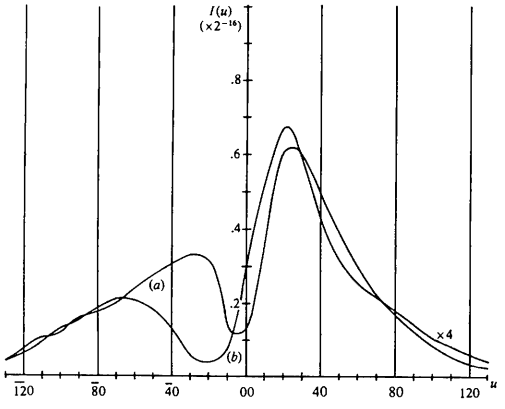

Fig. 11. Profile of dynamical factor for unit displacements in aluminum. Thicknesses (*a*) 12 Å and (*b*) 40 Å (*cf.* Fig. 7).

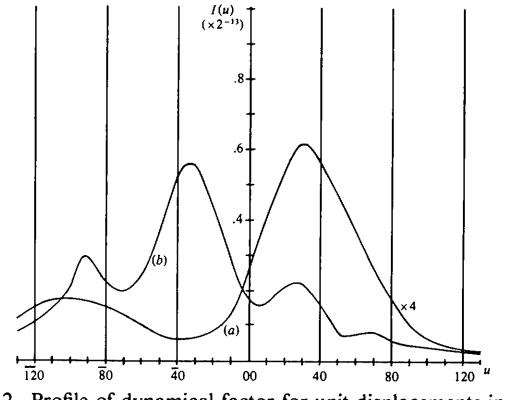

Fig. 12. Profile of dynamical factor for unit displacements in gold. Thicknesses (*a*) 12 Å and (*b*) 40 Å (*cf.* Fig. 8).

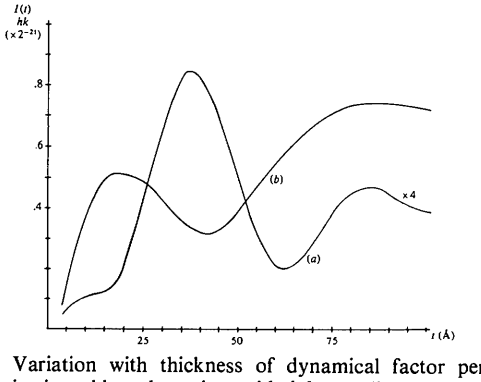

Fig. 14. Variation with thickness of dynamical factor per unit vacancies in gold at the points with *h*,*k* coordinates, relative to the superlattice unit cell, of 3,0 for curve (*a*) and 10,0 for curve (*b*) (*cf.* Figs. 6 and 10).

Images of split interstitials are much less dependent on crystal thickness than the diffraction pattern intensities under the conditions of our calculations. Although the image contrast may fluctuate, the form of the perturbation of the crystal remains recognizable at all thicknesses up to the range which is experimentally accessible. This result offers encouragement to the efforts to attain the necessary resolution capability with high-voltage electron microscopes.

Our model of a split interstitial in gold without lattice relaxation is not, of course, intended to represent a situation of immediate practical significance. It was chosen for the clarity of the images and diffraction effects and for computational convenience, to represent an extreme case of strong dynamical scattering effects.

The idea of using a 'dynamical factor' to represent the effect of dynamical scattering on diffuse intensity distributions in diffraction patterns was used by Fisher (1965). Having calculated the dynamical scattering intensities for a copper–gold alloy having an assumed degree of short-range ordering, he showed that the dynamical factor defined by the ratio $I_{\text{dyn}}/I_{\text{kin}}$ was a smoothly varying function so that the form of the diffuse scattering peaks was not seriously distorted by dynamical effects.

We have used a somewhat different concept. The 'dynamical factor' which we have defined is the function to be used in place of the kinematical scattering amplitude expression which multiplies the 'unitary' diffuse scattering expression, the second parts of the right-hand sides of equations (9) or (13). Our dynamical factors can thus be calculated in advance for a particular crystal of given orientation and thickness (or range of orientations and thicknesses) and can then be applied to obtain the diffuse scattering for any model for the defect correlations. The amount of computation required to deduce the dynamical factors with any accuracy is obviously quite large but is much less than would be required if the full dynamical calculation were made separately for each model of the defect correlation. Also, since to calculate dynamical factors it is necessary to consider only single, highly localized defects, the dimensions of the superlattice cells used in the periodic continuation calculations can be relatively small, of the order of two or three perfect-crystal unit-cell periodicities. To calculate intensities for a particular model involving defect correlations the superlattice unit-cell dimensions would have to be much greater than the range of the correlations and so would usually require the inclusion of a much greater number of diffracted beams.

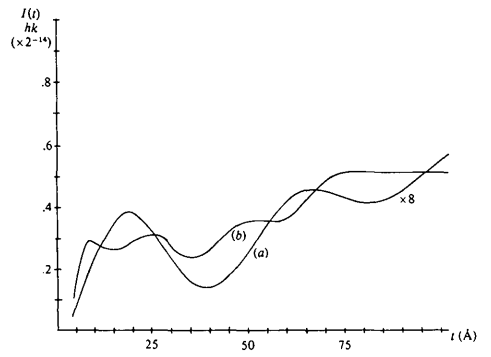

Fig. 16. Variation with thickness of dynamical factor for unit displacements in gold at points (*a*) 3,0 and (*b*) 10,0 (*cf.* Figs. 8 and 12).

An important limitation of our treatment is the assumption of kinematical scattering by the deviation from the perfect-crystal potential distribution in each slice. This approximation will break down to a significant extent for vacancies in heavy-atom materials such as gold or even for short-range ordering with large differences in the scattering amplitudes of the atoms, as in the case of copper–gold alloys (Cowley & Murray, 1968). A first-order correction to this approximation can be made at the expense of further complication of the computing. Thus, if a phase-object approximation is made, the scattering by a deviation in slice t of type n may be written (Cowley, 1975):

$$\mathscr{F}\exp\{-i\sigma\Delta\Phi_i^{n,t}(xy)\} = \delta(uv) - i\sigma\Delta\Phi_i^{n,t}(uv) - \tfrac{1}{2}\sigma^2\{\Delta\Phi_i^{n,t}(uv) * \Delta\Phi_i^{n,t}(uv)\} + \ldots, \quad (15)$$

so that $\Delta\Psi_k^{nt}(uv)$ in (11) is replaced by

$$\Delta\Psi_k^{n,t,1}(uv) - \Delta\Psi_k^{n,t,2}(uv) + \ldots, \quad (16)$$

where $\Delta\Psi_k^{n,t,2}(uv)$ is the change in the Fourier transform of the exit wave function derived from the second-order term of (15).

For a single defect type the dynamical factor summation in (13) is then replaced to a first approximation by

$$\sum_t \{|\Delta\Psi^{t,2}(\mathbf{u})|^2 + |\Delta\Psi^{t,2}(u)|^2 + 2\,\mathrm{Re}[\Delta\Psi^{t,1}(\mathbf{u}).\Delta\Psi^{t,2*}(u)]\}. \quad (17)$$

Thus this refinement requires that the number of multislice calculations be doubled. The result would be some modification of the forms of the dynamical factors but no essential change in the general conclusions to be drawn.

From the very limited selection from our calculated results, presented here, it is clear that the summing over thickness of the diffuse intensities gives a considerable smoothing of the dynamical factor. The fluctuations with thickness are damped much more rapidly than in the case of the scattering from a single defect. When the kinematical diffuse scattering from the unit defect is strongly anisotropic, as in the case of atomic displacements, the dynamical factor rapidly becomes more isotropic with increasing thickness. For single crystals

in the thickness range normally used for electron diffraction observations it appears likely that the dynamical factors will vary smoothly with thickness and will be very nearly isotropic except for Kikuchi-band effects. It should therefore be a good approximation to assume, as suggested earlier, that an atom displacement in any direction can be approximated by the sum of displacements in two perpendicular directions, or of displacements along any two near-orthogonal directions which seem appropriate.

The appearance of the strong Kikuchi-band or channelling patterns for gold (Fig. 6) is consistent with observational experience. In many cases the configuration of bands appears to modulate the diffuse scattering distribution due to defects or thermal vibrations without any distortion or masking of its characteristic features. The positions of the Kikuchi bands are strongly dependent on crystal orientation. Very thin crystals are commonly bent so that the Kikuchi bands are smeared out and are rarely seen.

We may conclude that for many cases of simple defect types the effects of dynamical scattering will be qualitatively represented by a modulation of the kinematical diffuse scattering distribution with a slowly varying dynamical factor function which is reasonably isotropic except for Kikuchi-band effects. For quantitative interpretation of the diffuse scattering, accurate calculation of the dynamical factor is possible, but laborious with present methods.

It must be emphasized that the dynamical factors for different types of unit defects will be widely and qualitatively different. Thus, as suggested earlier on the basis of a simple phase-object model (Cowley, 1965), dynamical effects are very different for displacement and replacement defects. This was confirmed by the observations and calculations of P. M. J. Fisher (private communication) who showed that, relative to the diffuse scattering due to short-range-order atom replacements in Cu–Au alloys, the asymmetric contributions to the diffuse peaks due to size-effect displacements are strongly suppressed when the incident beam is in a principal orientation. This difference has appeared also in our calculations for vacancies and displacements.

For a more complicated form of crystal defect, with correlations between atom site occupancies and atom displacements, as in short-range ordering with size effects or vacancies with lattice relaxation, the contributions of the final cross-product terms of (14) and similar terms, may add further complication. We have not, as yet, carried out the computations needed to suggest the form of these terms. However it is clear that these may add to the deviations from the form of the kinematical diffuse scattering due to the differences in the dynamical factors for the various types of unit defects considered separately. Obviously caution is indicated in the interpretation of diffuse scattering in electron diffraction patterns from non-trivial forms of defects until more complete calculations have provided detailed indications of the types of complications which may occur in the dynamical scattering effects.

This work was supported by NSF Grant DMR76-06108.

References

COWLEY, J. M. (1965). *Proc. Int. Conf. Electron Diffraction and the Nature of Defects in Crystals*, Melbourne, Australian Academy of Science, paper J-5.

COWLEY, J. M. (1971). *Advances in High Temperature Chemistry*. Vol. 3, edited by L. EYRING, pp. 36–85. New York: Academic Press.

COWLEY, J. M. (1975). *Diffraction Physics*. Amsterdam: North-Holland.

COWLEY, J. M. & MURRAY, R. J. (1968). *Acta Cryst.* A**24**, 329–336.

COWLEY, J. M. & POGANY, A. P. (1968). *Acta Cryst.* A**24**, 109–116.

DOYLE, P. A. (1969). *Acta Cryst.* A**25**, 569–577.

DOYLE, P. A. (1971). *Acta Cryst.* A**27**, 109–116.

FEJES, P. L., IIJIMA, S. & COWLEY, J. M. (1973). *Acta Cryst.* A**29**, 710–714.

FIELDS, P. M. & COWLEY, J. M. (1978). *Acta Cryst.* A**34**, 103–112.

FISHER, P. M. J. (1965). *Proc. Int. Conf. Electron Diffraction and the Nature of Defects in Crystals*, Melbourne, Australian Academy of Science, paper IH-4.

GJØNNES, J. (1966). *Acta Cryst.* **20**, 240–249.

GJØNNES, J. & WATANABE, D. (1966). *Acta Cryst.* **21**, 297–302.

HIRSCH, P. B., HOWIE, A., NICHOLSON, R. B., PASHLEY, D. W. & WHELAN, M. J. (1965). *Electron Microscopy of Thin Crystals*. London: Butterworths.

HOWIE, A. & BASINSKI, Z. S. (1968). *Philos. Mag.* **17**, 1039–1063.

IIJIMA, S. & O'KEEFE, M. A. (1979). In preparation.

KRAKOW, W. (1976). *Ultramicroscopy*, **1**, 203–221.

KUAN, T. S. & SASS, S. L. (1976). *Acta Metall.* **24**, 1053–1059.

SPENCE, J. C. H. (1978). *Acta Cryst.* A**34**, 112–116.

TAKAGI, S. (1962). *Acta Cryst.* **15**, 1311–1312.